Towards Automatic and Fast Annotation of Seismocardiogram Signals Using Machine Learning

Hiren Kumar Thakkar, *Member, IEEE*, and Prasan Kumar Sahoo, *Senior Member, IEEE*

***Abstract*—The automatic annotation of Seismocardiogram (SCG) potentially aid to estimate various cardiac health parameters continuously. However, the inter-subject variability of SCG poses great difficulties to automate its accurate annotation. The objective of the research is to design SCG peak retrieval methods on the top of the ensemble features extracted from the SCG morphology for the automatic annotation of SCG signals. The annotation scheme is formulated as a binary classification problem. Three binary classifiers such as Naïve Bayes (NB), Support Vector Machine (SVM), and Logistic Regression (LR) are employed for the annotation and the results are compared with the recent state-of-the-art schemes. The performance evaluation is carried out using 9000 SCG signals of 20 presumably healthy volunteers with no known serious cardiac abnormalities. The SCG signals are acquired from the Physionet public repository "cebsdb". The models are rigorously validated using metrics "Precision", "Recall", and "F-measure" followed by 5-fold cross-validation. The experimental validation with recent state-of-the-art solutions establishes the robustness of the proposed NB, SVM and LR with average annotation accuracy of 0.86, 0.925 and 0.935, respectively. The mean response time of proposed models is in the fraction of $\frac{1}{10}$ sec, which establishes its application for the real-time annotation.**

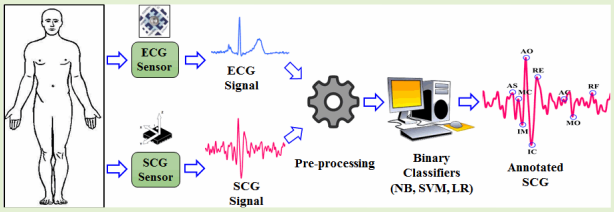

***Index Terms*—Seismocardiogram (SCG), automatic annotation, cardiac health parameters (CHPs), non-invasive, machine learning.**

I. Introduction

THE recent advancements in the field of sensing technology have made it possible to obtain the ultra-low vibrations from the chest surface produced by various cardiac mechanical events [1], [2]. The seismocardiogram (SCG) is one of the promising modalities that captures the cardiac events in the form of mechanical vibrations [3]. In a healthy subject, each SCG cardiac cycle exhibits up to nine individual mechanical events in the form of signal peaks as shown in Fig. 1. The SCG peaks and corresponding mechanical events [4] are described in Table I. The accurate annotation of the aforementioned nine SCG peaks enables the non-invasive detection of cardiac conditions such as early-stage hemorrhage [5], heartbeat performance [6], and ischemia [7].

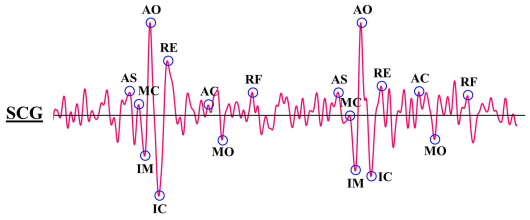

Fig. 1. Example annotation of SCG.

Nowadays, several Cardiac Health Parameters (CHPs) are employed to foresee the early signs of Cardiovascular Diseases (CVDs) such as Heart Rate Variability (HRV), Pulse Transit Time (PTT), Respiratory Phases (RP), Stroke Volume (SV), and Cardiac Time Intervals (CTIs). The Electrocardiogram (ECG) signals are well studied and numerous

Manuscript received September 30, 2019; accepted October 27, 2019. Date of publication November 1, 2019; date of current version February 5, 2020. This work was supported in part by the Ministry of Science and Technology (MOST), Taiwan, under Grant 107-2221-E-182-073 and Grant 108-2221-E-182-050 and in part by the Chang Gung Medical Foundation, Taiwan, under Grant CMRPD2H0291 and Grant CMRPD2J0141. The associate editor coordinating the review of this article and approving it for publication was Prof. Danilo Demarchi. *(Corresponding author: Prasan Kumar Sahoo.)*

H. K. Thakkar was with the Department of Computer Science and Information Engineering, Chang Gung University, Taoyuan 333, Taiwan. He is now with the Department of Computer Science Engineering, Bennett University, Greater Noida 201310, India (e-mail: hirenkumar.thakkar@bennett.edu.in).

P. K. Sahoo is with the Department of Computer Science and Information Engineering, Chang Gung University, Taoyuan 333, Taiwan, and also with the Division of Colon and Rectal Surgery, Chang Gung Memorial Hospital, Taoyuan 333, Taiwan (e-mail: pksahoo@mail.cgu.edu.tw).

Digital Object Identifier 10.1109/JSEN.2019.2951068

TABLE I
THE SET OF IMPORTANT SCG PEAKS WITH CORRESPONDING CARDIAC MECHANICAL ACTIVITIES

SCG peak	Mechanical activity	SCG peak	Mechanical activity
AS	Artial systole	IC	Isovolumic contraction
MC	Closing of mitral valve	RE	Rapid blood ejection
IM	Isovolumic movement	AC	Closing of aortic valve
AO	Aortic valve opening	MO	Mitral valve opening
RF	Rapid filling of blood		

approaches are available, which can estimate the CHPs using standalone ECG [8]. Recent studies show that Ballistocardiogram (BCG) and Seismocardiogram (SCG) are capable to estimate the CHPs in a standalone manner. However, BCG and SCG signals are not well studied and there is a lack of consensus on various feature points. Therefore, BCG and SCG are commonly used to estimate the CHPs in conjunction with ECG, Echocardiography (Echo), photoplethysmogram (PPG), etc., [9]. In the past few years, adequate progress is made in the direction of standalone use of SCG to estimate the CHPs such as estimation of CTIs [10], [11] and RP [12]. However, non-invasive and accurate estimation of other CHPs using standalone SCG requires further investigation. The non-invasive estimation of the aforementioned CHPs can be accomplished by analyzing the SCG signals. However, the estimation of CHPs from SCG requires an efficient method to annotate the specific important peaks.

A. Motivation

Contrary to Electrocardiogram (ECG), the SCG morphology is highly obscure and puzzling to comprehend. Typically, SCG signals vary from one subject to another and from one cardiac cycle to another. Moreover, body induced signal artifacts may contaminate SCG mechanical vibrations during the retrieval, which makes it challenging to accurately locate the desired peaks leading to the overall failure of the annotation. As shown in Fig. 1, peaks such as $\{AO, RE\}$ and $\{IM, IC\}$ exhibit the similar morphological amplitude, which makes it more complicated to distinguish the peaks during automatic annotation. Therefore, an efficient and responsive approach is required to tackle the dynamic nature of SCG signals for an automatic annotation. The fundamental shortcoming of the existing approaches is their lack of adaptability to tune the solution with the dynamic nature of error-prone SCG signals. Hence, it is highly essential to design a robust annotation scheme that learns the morphological behavior and automatically distinguish the set of desired peaks to that of undesired.

Rest of the paper is organized as follows. Section II presents the related works. The methodology is described in Section III. The Machine Learning (ML) classifiers are described in Section IV. The experiment dataset and performance metrics are described in Section V. The results are reported in Section VI followed by discussion in Section VII. The concluding remarks are made in Section VIII.

II. RELATED WORKS

The ECG, BCG, and SCG signals are considered as low-cost alternatives to monitor various cardiac health conditions of patients. In the past, several researchers have engaged ECG for the recognition of various cardiac health conditions [13], [14]. However, ECG exhibits merely five important peaks $\{P, Q, R, S, T\}$, which limits the in-depth analysis of cardiac activities. Hence, competitive cardiac signals such as BCG and SCG are explored to complement the ECG based cardiac health monitoring. However, a recent study gives SCG an edge over BCG [15].

Numerous SCG based applications are proposed to non-invasively monitor stroke volume, heart rate variability, and cardiac time intervals [16], [17]. To be specific, the aforementioned conditions are directly or indirectly estimated from the SCG important peaks. Hence, in the past few years, the research focus is largely shifted on the automatic annotation of specific SCG peaks without human involvement.

In [18], an approach to annotate SCG using high-frequency precordial accelerations is presented. Various envelops are designed using the source SCG signals to help annotate the SCG in turn. However, the proposed method does not provide a complete solution to successfully annotate all of the nine desired SCG peaks. Instead, envelops are designed to help annotate only two specific SCG peaks IM and IC.

In [11], an SCG peaks annotation (described as SCG fiducial points delineation) method is introduced to non-invasively estimate cardiac time intervals. Primarily three fiducial points are annotated such as IM, AO, and AC by designing three external envelopes from the source SCG itself. However, SCG morphology is highly complex and varies from one subject to another. Hence, it impacts the quality of envelope formation and thereby affects the overall delineation accuracy. Besides, the proposed method requires external envelope formation to delineate fiducial points, which increases the complexity of the solution. Moreover, only three fiducial points are delineated, which limits the applicability of the approach.

In [19], a sliding template-based systolic and diastolic peaks annotation method is proposed. The ensemble averaging of Cardiac Cycles (CCs) is carried to minimize the signal distortion. However, ensemble averaging may not help much to improve peak detection accuracy beyond a certain limit. The smoothen SCG may contain a set of potential candidate SCG peaks with morphological characteristics to that of the desired one. In the absence of a method that distinguishes the desired and undesired SCG peaks from signal morphology, the annotation process may end up annotating the wrong peaks, which may reduce the accuracy of estimated systolic time intervals.

In [20], an annotation method for gyroscope acquired SCG is presented. An additional gyroscope recording based rotational kinetic energy waveforms (RKEW) are employed for the annotation of SCG peaks IM and AC. However, the RKEW waveforms are derived from source SCG signals and hence the quality of derived RKEW waveforms are strongly dependent on the quality of underlying SCG signals.

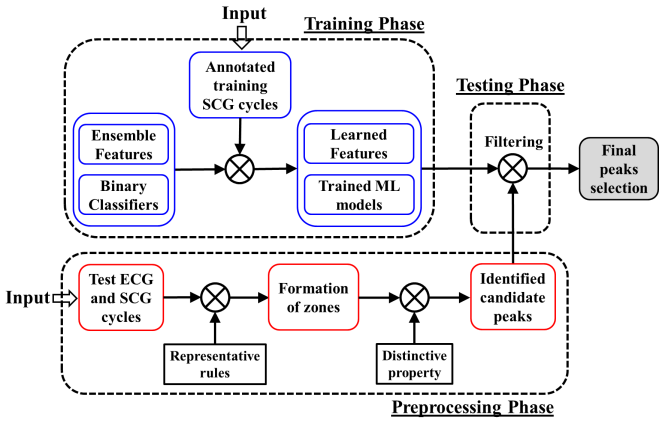

Fig. 2. Overview of SCG annotation framework.

In this paper, our goal is to design automatic annotation models for the SCG signals with a two-fold focus on the annotation accuracy and the response time. Further, the proposed annotation models attempt to identify all of the nine SCG peaks in Cardiac Cycles (CCs). Based on the goal, our contributions can be described as follow.

- We have designed a machine learning-based novel SCG annotation framework.
- We have designed three ensemble features extracted from the morphological knowledge of SCG.
- We have designed an efficient preprocessing mechanism comprised of zone formation and candidate peaks identification to help expedite the automatic annotation for continuous cardiac monitoring.
- We have formulated an SCG annotation as a binary classification problem and tackled by employing binary classifiers.

III. Methodology

In this section, we describe the fast and automatic annotation of the desired SCG peaks.

A. Overview of SCG Annotation Framework

The SCG annotation framework is broadly divided into three phases namely the preprocessing, training, and testing as shown in Fig. 2. During the training, classifiers are trained and ensemble features are learned. Before testing, preprocessing is carried out to identify candidate peaks. Finally, undesired candidate peaks are located and filtered out using trained classifiers in the testing phase. The detailed description of each phase is provided in subsequent sections.

B. Ensemble Features Designing

Three features namely *Amplitude*, *Time of appearance* and *Count* are derived from the morphological knowledge of SCG as described follow.

1) Amplitude: It represents the intensity of cardiac mechanical activity and takes $+ve$ or $-ve$ value. Each desired SCG peak corresponds to a specific cardiac mechanical activity and has a distinguishing amplitude behavior. For example, AO and AC corresponds to high $+ve$ and low $+ve$ amplitude, respectively. These morphological amplitude behaviors of peaks serve as a better predictor to improve the annotation. However, amplitude alone may not be sufficient to distinguish between the desired and undesired SCG peaks, and therefore other features are investigated.

2) Time of Appearance: In many instances, the amplitude of peak goes beyond its expected range, which makes it challenging to correctly distinguish between the adjacent peaks. For instance, a similar amplitude of MC and AO makes it challenging for an algorithm to distinguish between them. Therefore, a novel feature named *Time of appearance* is designed. Unlike amplitude, the time of appearance of SCG peaks is observed to be more consistent in the time domain. Besides, peaks appear in predefined sequential order such as MC followed by AS, IM followed by MC etc. The pseudo-accurate nature of peaks in the time domain is tapped and used as an additional measure to effectively identify the desired peaks.

The *Time of appearance* for each peak is calculated as follows. For AO, the *Time of appearance* is measured for QRS of the concurrent ECG cycle, which usually takes the $+ve$ value. For others, *Time of appearance* is measured for AO. For example, peaks appearing before AO are assigned with $-ve$ value and those appearing after AO are assigned with $+ve$ value in each cycle.

3) Count: When two or more peaks have similar amplitude and are very close to each other in the time domain, it becomes challenging for the automatic annotation models to pick the desired one based on the *Amplitude* and the *Time of appearance*. Hence, the third feature namely *Count* is incorporated to complement their limitations. The *Count* is defined as the number of Upslopes and Downslopes away a particular SCG peak from AO. As reported in [21], SCG peaks are separated by a certain number of Upslopes and Downslopes. For example, IM is one Downslope away from MC, and AO is one Upslope away from IM as shown in Fig. 1. Learning the representative value of *Count* for all peaks with respect to AO may help to distinguish peaks successfully that are very close to each other and have similar amplitude.

The ensemble features' extraction and their corresponding representative value estimation is carried out over the ensemble average of $K = 12$ training cardiac cycles. Here, $K = 12$ is obtained experimentally, which gives better results.

C. Preprocessing of SCG Signals

In preprocessing, each SCG cycle is divided into three zones to reduce the search area. Subsequently, distinctive properties described in Table II are employed to expedite the identification of potential candidate peaks.

1) Zones Formation: The SCG cycle can be partitioned into three zones concerning ECG as shown in Fig. 3. The zones are formulated by comparing the morphology of SCG to that of the concurrent ECG. In a healthy subject, the Wiggers diagram [22] along with the recent studies [11], [19] confirm

TABLE II
SCG PEAKS WITH DISTINCTIVE CHARACTERISTICS

SCG Peak	Representative rule with respect to ECG	Distinctive property
AS	Between offset of P wave and onset of QRS	max_peak
MC	Between onset of QRS and T wave	max_peak
IM	Between onset of QRS and T wave	min_peak
IC	Between onset of QRS and T wave	min_peak
RE	Between onset of QRS and T wave	max_peak
AC	Between offset of T and onset of subsequent P wave	max_peak
MO	Between offset of T and onset of subsequent P wave	min_peak
RF	Between offset of T and onset of subsequent P wave	max_peak

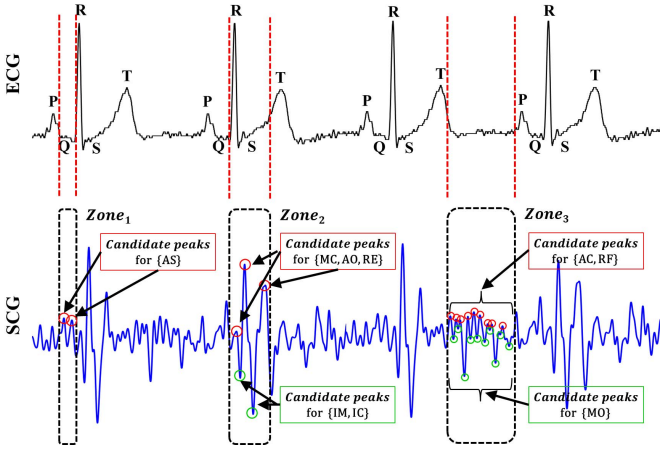

Fig. 3. The zones formation and candidate peaks identification.

that the cardiac electrical and mechanical events take place in a well-defined sequence that appear concurrently in ECG and SCG, respectively. In the systolic profile of ECG, i.e., the onset of QRS to offset of T, the ventricle pressure rapidly increases and then decreases after attaining the maximum level leading to the cardiac mechanical activities such as MC, AO, IM, IC, and RE in SCG. Therefore, Zone 2 is formulated concerning the systolic profile of ECG. Similarly, Zone 1 and Zone 3 are formulated concerning the diastolic profile of ECG, i.e., offset of T to the onset of QRS. The diastolic profile initiates the closure of the Aortic valve (AC) and concludes with the opening of Mitral valve (MO) represented as Zone 3 followed by the atrial systole, i.e., offset of P to the onset of QRS in ECG represented as Zone 1.

Three knowledge-based representative rules are formulated to form zones as summarized in Table II. The representative rules are defined as follows.

Representative rule-1: Align the ECG time duration between offset of P wave and onset of QRS to the concurrent SCG to form $Zone_1$ for the discovery of AS.

Representative rule-2: Align the ECG time duration between onset of QRS and onset of T wave to the concurrent SCG to form $Zone_2$ for the discovery of MC, IM, IC, and RE.

Representative rule-3: Align the ECG time duration between offset of T wave and onset of subsequent cycle's P wave to the concurrent SCG to form $Zone_3$ for the discovery of AC, MO, and RF.

2) Identification of Candidate Peaks: In each zone, maxima and minima are located as potential candidate peaks. However, only the subset of potential candidate peaks are chosen as candidate peaks using the distinctive properties as summarized in Table II. For example, as shown in Fig. 3, AS has a distinctive property of being maxima represented as `max_peak`. Hence, only the set of maxima are considered as candidate peaks of AS in $Zone_1$ as shown in Fig. 3. Similar process is followed for the $Zone_2$ and $Zone_3$. The process of choosing the subset of candidate peaks out of the set of potential candidate peaks further accelerates the annotation process by reducing the search space.

IV. MACHINE LEARNING CLASSIFIERS

The SCG signals from the real subjects vary from one subject to another, which make it challenging to annotate the desired peaks. Therefore machine learning classifiers are employed to capture the morphological changes in signals and to generalize the signal behavior.

A. Classifiers Selection

Since our primary objective is to perform the automatic annotation in a real-time and continuous manner, complex classifiers may not serve the purpose. Classifier such as Artificial Neural Networks (ANN) requires greater computational power as well as time to tune several parameters. On the contrary, the decision tree, boosted tree, and random forest classifiers require optimum splitting rules with the size of output tree as minimum as possible, which is challenging to accomplish in a time-efficient manner given the fluctuations in input SCG. Besides, classifiers such as K-Nearest Neighbors (KNN), ANN, and decision tree are not a good fit to analyze time-series data such as SCG and are prone to overfitting. The KNN, ANN, and decision tree are more flexible and therefore are subject to high variance leading to cause major fluctuations in the prediction model with the changes in input training data.

The NB, SVM, and LR are exclusively chosen as they are less computer-intensive and highly robust against the overfitting, which makes them suitable to apply for real-time monitoring. The NB and LR have low variance and prediction models built on top of them are more tolerant with the underlying change in input training data. Besides, NB, SVM, and LR require only a few parameters to tune, which is ideal for quick learning and annotation.

B. Naïve Bayes (NB) Classifier

Let $SCGPs = \{AS, MC, IM, IC, RE, AC, MO, RF\}$ be the set of desired SCG peaks. For any $x \in SCGPs$, let us assume that n candidate peaks are identified represented as $CP_x = \{cp_x^1, cp_x^2, \ldots, cp_x^n\}$. The objective is to classify each $cp_x^i \in CP_x$ into either of two classes C_k, $k \in \{1, 2\}$, where C_1 and C_2 represents the class *selected* and *rejected*, respectively. For each cp_x^i, a feature vector $F_x^i = \{C_x^i, T_x^i, A_x^i\}$ is prepared as shown in Table III. Here, C_x^i, T_x^i, and A_x^i represents the feature *Count, Time of appearance*, and *Amplitude* of i^{th} candidate peak of the desired SCG peak x, respectively. Using F_x^i, the conditional probabilities $p(C_1|F_x^i)$ and $p(C_2|F_x^i)$ can

TABLE III
SCG FEATURE NOTATIONS

Notation	Meaning
C_x^i	Count of i^{th} candidate of peak x.
T_x^i	Time of appearance of i^{th} candidate of peak x.
A_x^i	Amplitude of i^{th} candidate of peak x.

$x \in SCGPs = \{AS, MC, IM, IC, RE, AC, MO, RF\}$, $i = \{1, 2, ..\}$

be modelled as shown in Eq. 1.

$$p(C_k|F_x^i) = p(C_k|C_x^i, T_x^i, A_x^i), \quad k \in \{1, 2\}, \ i \in \{1, 2, \ldots, n\} \tag{1}$$

The C_x^i, T_x^i and A_x^i are conditionally independent to each other. Hence, we can rewrite Eq. 1 as shown in Eq. 2.

$$p(C_k|C_x^i, T_x^i, A_x^i) \propto p(C_k) \times p(C_x^i|C_k) \times p(T_x^i|C_k) \times p(A_x^i|C_k) \tag{2}$$

Here, $p(C_x^i|C_k)$, $p(T_x^i|C_k)$ and $p(A_x^i|C_k)$ represents the probability of C_x^i, T_x^i, and A_x^i for a given class C_k, respectively.

The μ_{k,C_x}, μ_{k,T_x}, and μ_{k,A_x} are mean of features *Count, Time of appearance*, and *Amplitude* for a given SCG peak x and class C_k, respectively. Similarly, σ^2_{k,C_x}, σ^2_{k,T_x}, and σ^2_{k,A_x} are the standard variance of *Count, Time of appearance* and *Amplitude* for a given SCG peak x and class C_k, respectively. The mean $\{\mu_{k,C_x}, \mu_{k,T_x}, \mu_{k,A_x}\}$ and standard variance $\{\sigma^2_{k,C_x}, \sigma^2_{k,T_x}, \sigma^2_{k,A_x}\}$ are the learning parameters estimated from the training samples of class C_k.

A binary Naïve Bayes classifier can be constructed on the top of the model by incorporating Maximum a Posteriori (MAP) decision rule. The classifier function assigns a class label $\widehat{y} = C_k$ for $k \in \{1, 2\}$ as shown in Eq. 3.

$$\widehat{y} = \underset{k \in \{1,2\}}{\text{argmax}}\, p(C_k) \prod_{j=1}^{|F_x^i|} p(f_j|C_k), \quad where \ f_j \in \{C_x^i, T_x^i, A_x^i\} \tag{3}$$

The candidate peaks have equal probability to be selected as well as rejected. Hence, prior probability distribution is assumed equiprobable with $p(C_1) = p(C_2) = \frac{1}{\#\ of\ classes} = 0.5$.

$$x = max\left(p(C_1|cp_x^1), \ p(C_1|cp_x^2), \ldots, \ p(C_1|cp_x^n)\right) \tag{4}$$

If more than one candidate peaks are classified as *selected* with class label $\widehat{y} = C_1$, the cp_x^i with Maximum Likelihood Probability (MLP) for class C_1 (*e.g., selected*) is chosen as the desired SCG peak x as shown in Eq. 4.

C. Support Vector Classifier

In this section, supervised non-probabilistic binary classifier is designed to classify the candidate peaks into class *selected* or *rejected*. For each SCG peak $x \in SCGPs$, the SVM is trained to construct the classification hyperplane. Let us say for any SCG peak $x \in SCGPs$, there are m linearly separable labelled training samples in data set $Z_x = \{(z_x^1, y_x^1), (z_x^2, y_x^2), \ldots, (z_x^m, y_x^m)\}$, where $m > 0$. Here, $z_x^i \in Z_x$ is i^{th} training peak of desired SCG peak x consisting of feature vector $F_x^i = \{C_x^i, T_x^i, A_x^i\}$, and $y_x^i \in Z_x$ is the class label for i^{th} training peak of desired SCG peak x. The $y_x^i = +1$ and $y_x^i = -1$ represents class *selected* and *rejected*, respectively. The objective is to derive an optimum classification hyperplane that partitions the Z_x into two subsets, 1). The subset *selected* represented as $Z_x^{+1} = \{z_x^i \in Z_x | y_x^i = +1\}$, and 2). The subset *rejected* represented as $Z_x^{-1} = \{z_x^i \in Z_x | y_x^i = -1\}$, where $Z_x^{+1} \cap Z_x^{-1} = null$.

The linear SVM classifier represented by $\Phi_{w,b}(z_x^i)$ can be defined as shown in Eq. 5.

$$\Phi_{w,b}(z_x^i) = w^T F_x^i + b, \quad \forall z_x^i \in Z_x \tag{5}$$

Here, $\Phi_{w,b}(z_x^i)$ is a classification hyperplane, w is a weight vector, and b is a bias. The w is a learning vector, which is trained using the Z_x.

For the binary classification, three hyper-planes are defined, 1). The optimum hyperplane $\Phi_{w,b}(z_x^i) = w^T F_x^i + b = 0$. 2). The hyperplane for the class *selected* ($y_x^i = +1$) represented as $\Phi_{w,b}(z_x^i) = w^T F_x^i + b = +1$, and 3). The hyperplane for the class *rejected* ($y_x^i = -1$) represented as $\Phi_{w,b}(z_x^i) = w^T F_x^i + b = -1$. The distance between $\Phi_{w,b}(z_x^i) = +1$ and $\Phi_{w,b}(z_x^i) = -1$ is defined as $\frac{2}{||w||}$ and it is maximized under the constraint $y_x^i(w^T F_x^i + b) \geq 1$, for each $z_x^i \in Z_x$.

For the non-linearly separable training samples, the SVM is extended to include the hinge loss function $max(0, 1 - y_x^i(w^T F_x^i + b))$. In this case, the optimization problem can be defined as shown in Eq. 6, where λ decides the margin size and at the same time λ ensures that the sample $z_x^i \in Z_x$ lies in the correct class.

$$min\left(\left[\frac{1}{m}\sum_{i=1}^{m} max(0, 1 - y_x^i(w^T F_x^i + b))\right] + \lambda||w||^2\right), \quad where\ m = number\ of\ samples \tag{6}$$

The trained SVM is used to classify the $CP_x = \{cp_x^1, cp_x^2, \ldots, cp_x^n\}$. The candidate peak $cp_x^i \in CP_x$ that classifies into class *selected* (+1) is considered as a desired SCG peak x. If more than one candidate peaks are classified into class *selected*, the one with maximum distance from $\Phi_{w,b}(z_x^i) = 0$ is considered, as it has the least generalization error.

D. Logistic Regression (LR) Classifier

Let us assume that for an SCG peak $x \in SCGPs$, the set $Z_x = \{z_x^i | i = 1, 2, \ldots, k\}$ with k training data samples is available, where $z_x^i \in Z_x$ is an i^{th} training data sample. Each training sample z_x^i is comprised of feature vector $F_x^i = \{C_x^i, T_x^i, A_x^i\}$. A logistic linear function $\mathcal{L}(z_x^i)$ can be defined as shown in Eq. 7.

$$\begin{aligned}\mathcal{L}(z_x^i) &= \beta_0 + (\beta_1 \times C_x^i) + (\beta_2 \times T_x^i) + (\beta_3 \times A_x^i) \\ &= \beta^T \times F_x^i, \ \forall z_x^i \in Z_x\end{aligned} \tag{7}$$

Here, β_0, β_1, β_2 and β_3 are the classifier-specific learning parameters.

$$\sigma(\mathcal{L}(z_x^i)) = \sigma(\beta^T F_x^i) = \frac{1}{1 + exp^{-(\beta^T F_x^i)}} \tag{8}$$

Let us consider that there are n test data samples (i.e., candidate peaks) for an SCG peak x, which is represented as $CP_x = \{cp_x^1, cp_x^2, \ldots, cp_x^n\}$. For each candidate peak $cp_x^i \in CP_x$, the trained logistic regression model defined in Eq. 8 is used to predict the likelihood of cp_x^i to be classified in class *selected* as defined in Eq. 9.

$$\begin{aligned} p(selected|cp_x^i) &= \sigma(\mathcal{L}(cp_x^i)) = \sigma(\beta^T F_x^i) \\ &= \frac{1}{1 + exp^{-(\beta_0 + \beta_1 C_x^i + \beta_2 T_x^i + \beta_3 A_x^i)}} \end{aligned} \tag{9}$$

Out of the n candidate peaks, the one with maximum likelihood to be classified in a class *selected* is chosen as desired SCG peak x as shown in Eq. 10.

$$x = max\Big(p(selected|cp_x^1), p(selected|cp_x^2), .., p(selected|cp_x^n)\Big) \tag{10}$$

V. Dataset and Performance Metrics

A. Dataset Description

The combined measurement of ECG and SCG of twenty subjects is obtained from the Physionet public repository "cebsdb" [23], [24]. The subjects are presumably healthy volunteers with no serious cardiac abnormalities. The signals were acquired using a Biopac MP36 data acquisition system (Santa Barbara, CA, USA) and a triaxial accelerometer (LIS344ALH, ST Microelectronics) with bandwidth between 0.5 Hz and 100 Hz. The ECG measurement was carried out using electrodes with foam tape and sticky gel (3M Red Dot 2560). The sampling rate was 5 kHz. During the entire data acquisition process, the subjects were asked to be very still in a supine position on a comfortable conventional single bed and awake. For the analysis, dorso-ventral (i.e., z-axis) component of the 3-D SCG signal is used with positive polarity [25]. The demographic information of the subjects is presented in Table IV. The mean age of the subjects is 24.45 years. Out of 20 subjects, 12 are male and 8 are female.

The selection of the inertial sensor such as triaxial accelerometer (LIS344ALH) plays a significant role in overall system performance. Factors such as accelerometer range, sensitivity, noise density, surface area, number of axes of inertial sensor plays an important role in deciding the signal quality and subsequently the system performance. For instance, vibrations beyond the sensing range, i.e., maximum allowed amplitude get distorted and is clipped in output. Similarly, low sensitivity accelerometers unable to capture the ultra-low heart induced vibrations. Therefore, accelerometers need to be chosen carefully to acquire the quality signals. Although, there is no well defined minimum requirements available in the literature for accelerometer selection, the standards such as sensitivity up to 0.164 $\mu s/\mu g$, measurement range of $\pm$2g to $\pm$6g, and a noise density below 6.5 $\mu g/\sqrt{Hz}$ are proven to provide high quality signals with a resolution of up to 9 bits.

TABLE IV
SCG Dataset Description

Subjects	Gender	Age	Life style	Smoking	Coffee
S_1	Male	30	Sedentary	N	Y
S_2	Female	28	Healthy	N	Y
S_3	Female	25	Sedentary	N	Y
...	...	...	...	...	...
S_{20}	Female	26	Sedentary	N	Y

A unique **C**ardiac **C**ycle **Q**uality **I**ndex ($CCQI$) between 0 and 1 is derived as defined in Eq. 11 depending on the difficulty in annotation and the number of successfully annotated peaks.

$$CCQI = TS \times \frac{\#\ of\ successfully\ annotated\ SCG\ Peaks}{Total\ \#\ of\ SCG\ Peaks} \tag{11}$$

The TS is a triviality score assigned by expert annotators. The $TS = 1$ indicates the easy annotation and clear morphology; whereas $TS = 0$ indicates the challenging annotation and complex morphology. Finally, the CCs with Average Cardiac Cycle Quality Index (i.e., Avg_CCQI) more than 0.5 are considered for the experiment. The Avg_CCQI is defined in Eq. 12.

$$Avg\_CCQI = \frac{\sum_{i=1}^{n} CCQI_i}{n} \tag{12}$$

The n represents the number of expert annotators. In our experiment, $n = 2$ expert annotators are involved to validate any SCG peak and conflicts are resolved with the opinion of the third expert annotator. The quality of expert annotation is ensured using the inter-annotator kappa coefficient (κ) [26]. The annotation process concludes $\kappa = 0.73 \in (0.6, 0.8)$, which indicates a substantial agreement.

The summary of training, testing, and validation data set is as follows. Total 9000 CCs are randomly chosen from 20 subjects, i.e., 450 CCs per subject for the experimental purpose. Out of 9000 CCs, 6000 CCs are randomly chosen from 14 random subjects, i.e., 8 male and 6 female for the training and rest 3000 CCs, i.e., 4 males and 2 females are held out for the testing purpose. It is to be noted that the testing CCs are used for the model evaluation purpose only and are not involved in the training. 5-fold cross-validation is performed in our experiment and the set of 9000 CCs is randomly divided into five subsets of 1800 CCs each. In each fold, one subset of 1800 CCs is considered for the evaluation purpose and the rest four subsets that comprise 7200 CCs are used for the model training. The accuracy evaluation results are obtained based on the performance of the models on the validation data set of 1800 CCs.

The outcome of the expert annotation is summarized in Table V. For each SCG peak $x \in SCGPs = \{AS, MC, IM, IC, RE, AC, MO, RF\}$, the Table V shows the number of training CCs with valid annotation of a respective peak by both expert annotators. It is to note that not all 6000 CCs contain all of the nine important SCG peaks.

TABLE V
NUMBER OF TRAINING CARDIAC CYCLES (CCS) PER PEAK

AS	MC	IM	AO	IC	RE	AC	MO	RF
5244	5489	5621	5729	5553	5429	5143	5246	5286

The absence of any important peak in a CC justifies the presence of external signal artifacts. For each SCG peak $x \in SCGPs$, the proposed classifiers are trained and the features are estimated using training CCs.

B. Performance Metrics

The performance metrics such as Precision, Recall, and F-measure are employed for the quantitative accuracy evaluation. For the qualitative accuracy evaluation, Time Difference Error (TDE) and Time Difference Root Mean Square Error (TDRMSE) are considered as defined in Eq. 13 and 14, respectively.

$$TDE = |Timestamp_{R_{SCGP}} - Timestamp_{S_{SCGP}}| \quad (13)$$

$$TDRMSE = \sqrt{\frac{1}{q}\sum_{j=1}^{q}(TDE_x^j)^2}, \quad x \in SCGPs \quad (14)$$

The TDE represents the $Timestamp$ difference between the R_{SCGP} and the corresponding S_{SCGP}. For each SCG peak $x \in SCGPs$, the TDRMSE represents the average TDE over the q CCs under consideration. The accuracy assessment of various cardiac time intervals such as ST, DT, PEP and $LVET$ is performed by measuring the mean time interval difference between the expert and automatic estimation across q CCs as defined in Eq. 15.

$$MeanError(CTI^y) = \frac{\sum_{j=1}^{q}|T_{Expert}^{y,j} - T_{Auto}^{y,j}|}{q}, \quad where,\ y \in \{ST, DT, PEP, LVET\} \quad (15)$$

The $T_{Expert}^{y,j}$ and $T_{Auto}^{y,j}$ are expert and automatic time interval of y^{th} cardiac time interval observed in j^{th} CC, respectively. To evaluate the applicability of proposed models for real-time and continuous monitoring, Mean Response Time (MeanRT) is calculated across q CCs as defined in Eq. 16.

$$MeanRT^m = \frac{\sum_{j=1}^{q}|T_{Termination}^{m,j} - T_{Initiation}^{m,j}|}{q}, \quad where,\ m \in \{NB,\ SVM,\ LR\} \quad (16)$$

The $T_{Termination}^{m,j}$ and $T_{Initiation}^{m,j}$ represents the termination time and initiation time of the annotation process, respectively for j^{th} CC and m^{th} annotation model.

VI. RESULTS

The proposed models are trained on the training data set and are validated using a 5-fold cross-validation across the quantitative and qualitative performance metrics as discussed in Section V-B. On the contrary, the unbiased performance evaluation of the proposed model is provided by employing the test data set to validate the testing using the same quantitative and qualitative performance metrics.

TABLE VI
COMMONLY APPEARING VALUE OF FEATURES WITH RESPECT TO *AO*

SCG peak	Count	Time of appearance (sec)	Amplitude
AS	-4	-0.128 ± 0.0037	0.27 ± 1.65
MC	-2	-0.047 ± 0.01	16.6 ± 5.6
IM	-1	-0.024 ± 0.0035	-32.01 ± 1.921
IC	1	0.049 ± 0.0031	-24.26 ± 1.77
RE	2	0.069 ± 0.0037	6.12 ± 2.92
AC	10	0.18 ± 0.0074	0.94 ± 1.31
MO	13	0.22 ± 0.0056	-1.78 ± 1.60
RF	18	0.28 ± 0.010	2.59 ± 1.50

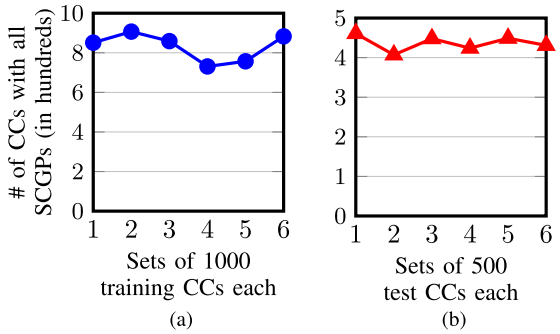

Fig. 4. The # of CCs with all of the nine SCG peaks (SCGPs).

A. Results of Expert Annotation

The results of the expert annotation are summarized in Table VI. The mean value of *Count*, *Time of appearance*, and *Amplitude* is derived from the training CCs.

As shown in Table VI, AS with $Count = -4$ indicates that AS normally appears four slopes (Upslopes and Downslopes) before the appearance of AO. The RF with $Count = 18$ indicates that RF is expected to appear eighteen slopes after the appearance of AO. Similarly, *Time of appearance* is obtained. For example, IC appears on an average $0.049 \pm 0.0031\ sec$ after the appearance of AO. Finally, the *Amplitude* -24.26 ± 1.77 of IC represents the mean amplitude observed for the expert annotation.

The training and testing CCs are separately annotated by expert annotators to locate the set of nine desired SCG peaks.

In Fig. 4a, the $x-axis$ shows the six sets of 1000 training CCs, and $y-axis$ shows the number of CCs exhibiting all of the nine SCG peaks. Similarly, Fig. 4b shows the outcome of the test set using the six sets of 500 CCs each. From Fig. 4, it is clear that significant number of training as well as testing CCs contain all of the nine SCG peaks and there is a consistency across the sets. Fig. 5 presents the extended outcome of Fig. 4a for each desired SCG peak.

B. Results of Proposed Classifiers

The proposed classifiers are implemented using a scikit-learn machine learning library [27]. Fig. 6 shows the annotation results of NB, SVM, and LR represented as NB_S_{SCGPs}, SVM_S_{SCGPs}, and LR_S_{SCGPs} with respect to expert annotation outcome R_{SCGPs}. The comparison of each desired SCG peak is carried out across six sets of 500 test CCs each. For each SCG peak, the set of R_{SCGPs} and S_{SCGPs} are plotted

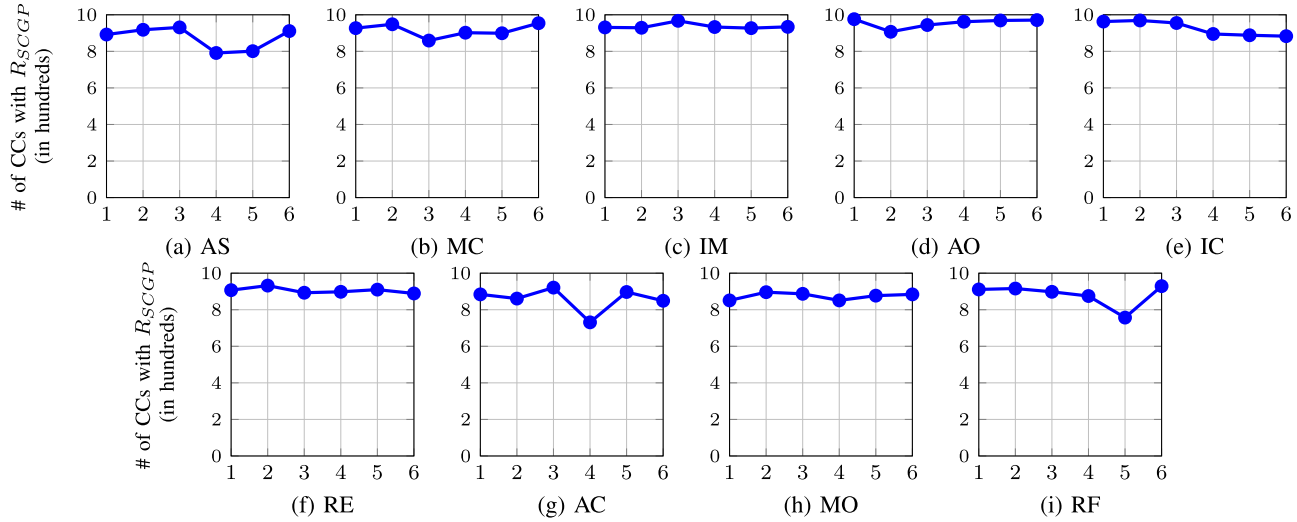

Fig. 5. Outcome of expert annotation representing the number of CCs with relevant SCG peak R_{SCGP} (a) AS, (b) MC, (c) IM, (d) AO, (e) IC, (f) RE, (g) AC, (h) MO, and (i) RF with respect to six sets of 1000 training CCs each.

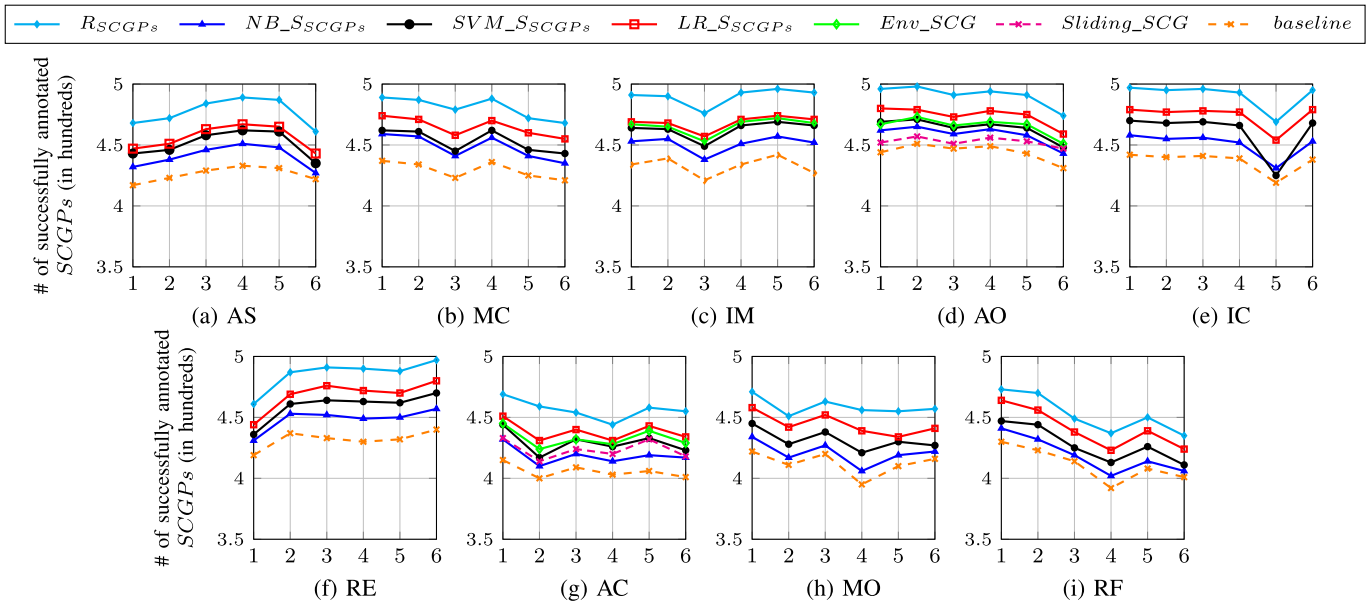

Fig. 6. Comparison of Selected SCG Peaks S_{SCGPs} of Naïve Bayes (NB_S_{SCGPs}), Support Vector Machine (SVM_S_{SCGPs}), and Logistic Regression (LR_S_{SCGPs}) with S_{SCGPs} of *Env_SCG*, *Sliding_SCG*, *baseline*, and with Relevant SCG peaks R_{SCGPs} of expert annotation for (a) AS, (b) MC, (c) IM, (d) AO, (e) IC, (f) RE, (g) AC, (h) MO, and (i) RF with respect to six sets of 500 testing CCs each.

across sets of 500 CCs each. The outcome trend reveals that proposed classifiers consistently follows the performance of the expert annotation. It is evident from Fig. 6 that similar to training CCs, AO is successfully annotated in most test CCs by the automatic and expert annotation.

The outcomes of proposed classifiers are also compared with the state-of-the-art recent annotation schemes Env_SCG [11], and $Sliding\_SCG$ [19] along with the baseline approach. The Env_SCG [11] is an envelope based scheme and focuses to annotate IM, AO, and AC; whereas $Sliding\_SCG$ is sliding window based scheme and focuses to annotate AO and AC. The proposed models are also compared with the *baseline* annotation model. From Fig. 6, it is clear that Env_SCG [11] performs marginally better compared to $Sliding\_SCG$ [19], *baseline* and proposed NB_S_{SCGPs}. In addition, Fig. 6 shows that the performance of LR is marginally better as compared to NB and SVM. For each SCG peak, LR has successfully identified and annotated more number of desired SCG peaks as compared to that of NB and SVM.

1) Results of Quantitative Accuracy Evaluation: The quantitative accuracy evaluation results are shown in Fig. 7 for NB, SVM, and LR for Precision, Recall, and F-measure. The results obtained for testing datasets are considered as input to calculate quantitative performance metrics. The results are compared with Env_SCG [11], $Sliding\_SCG$ [19], and *baseline*. From Fig. 7, it is clear that for the test dataset of 3000 CCs, LR outperforms over SVM and NB together with Env_SCG [11], $Sliding\_SCG$ [19], and *baseline* with respect to Precision and F-measure. It is also clear that with the increase in the number of testing CCs, the quantitative

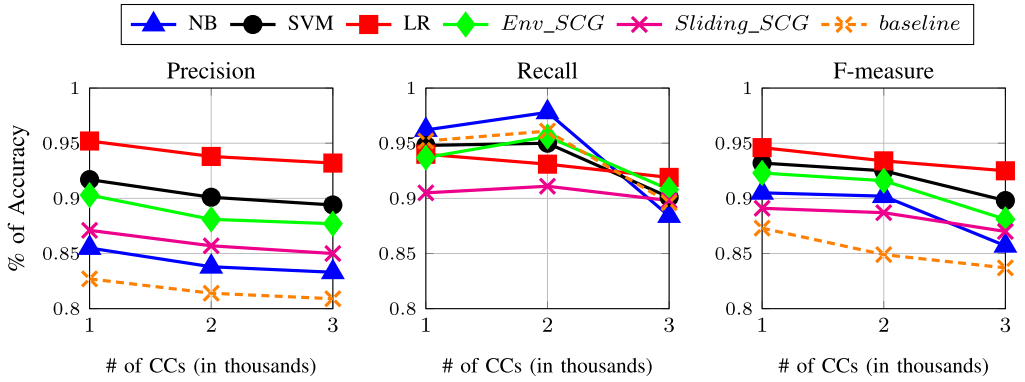

Fig. 7. Accuracy outcome comparison of proposed ML classifiers, NB, SVM, and LR with *Env_SCG*, *Sliding_SCG*, and *baseline* with respect to Precision, Recall and F-Measure for the testing dataset.

TABLE VII
COMMONLY APPEARING VALUE OF FEATURES WITH RESPECT TO *AO*

Model	fold 1	fold 2	fold 3	fold 4	fold 5	Mean accuracy
LR	0.917	0.903	0.911	0.884	0.881	0.899
SVM	0.836	0.841	0.832	0.875	0.883	0.853
NB	0.809	0.815	0.819	0.83	0.822	0.819
Env_SCG	0.846	0.851	0.868	0.838	0.83	0.847
Sliding_SCG	0.823	0.818	0.814	0.811	0.839	0.821
baseline	0.786	0.792	0.763	0.771	0.802	0.783

accuracy decreases marginally for all annotation schemes. It is to note that F-measure is a single value performance indicator and is a combined representation of Precision and Recall. The average accuracy of NB, SVM, and LR is 0.86, 0.925, and 0.935, respectively with respect to F-measure. Compared to the external envelopes employed in Env_SCG [11], the proposed classifiers benefit from the zone formation, which results in better estimation of the probable search area for various peaks. Moreover, we consider the distinctive properties, which minimizes the search process and thereby reduces the instances of the wrong annotation between closely appeared morphologically similar peaks. To be specific, contrary to Env_SCG [11], the proposed classifiers are better equipped with pre-processing and have a more accurate and concise search area.

Further, the performance reliability of the models is ensured using the 5-fold cross-validation. The results of 5-fold cross-validation are reported in Table VII. The 5-fold cross-validation results establish the robustness of the proposed models. The accuracy evaluation results of the 5-fold cross-validation are more reliable as they are obtained based on the extensive evaluation of the models on a different subset of unseen test cycles in each fold. On the line of our earlier results reported in Fig 6 and 7, the 5-fold cross-validation confirms the superiority of LR over others. Besides, it is also confirmed that the NB shows consistently poor performance during 5-fold cross-validation.

2) Results of Qualitative Accuracy Evaluation: The quantitative accuracy evaluation results establish that binary classifiers are well suit to tackle the time-series unobtrusive SCG annotations.

The qualitative accuracy evaluation results of the proposed annotation models are obtained using performance metrics

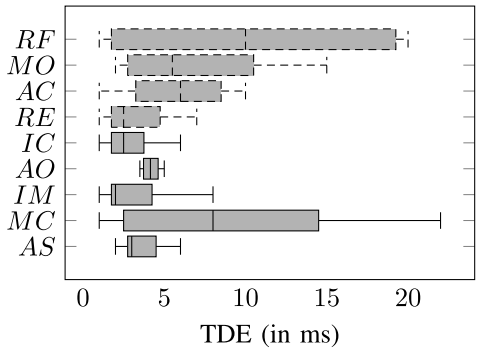

Fig. 8. Accuracy evaluation results with respect to Time Difference Error (TDE) for the test dataset.

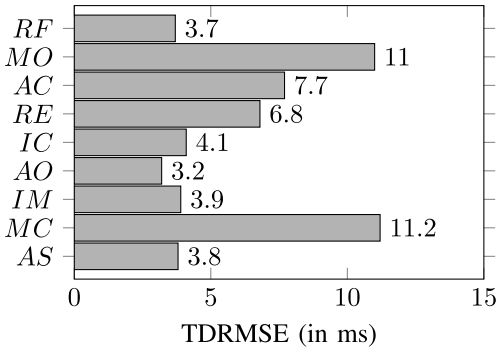

Fig. 9. Accuracy evaluation results with respect to the Time Difference Root Mean Square Error (TDRMSE) for the testing dataset.

such as TDE and TDRMSE as presented in Fig. 8 and Fig. 9, respectively. For each desired SCG peak, Fig. 8 presents the box plot to show three resultant outcomes such as median TDE (in ms), maximum TDE, and minimum TDE between the proposed and expert annotation approaches. From Fig. 8, it is clear that IM has the least median TDE and RF has the maximum TDE. Moreover, in Fig. 6, it is also clear that although AO has marginally more median TDE, the difference between its maximum and minimum TDE is least among others. The possible explanation of improved qualitative accuracy results of AO lies in its convenient retrieval by experts as well as proposed annotation classifiers as shown in Fig. 6. For the robust accuracy evaluation, in addition to the Time Difference Error (TDE), the Time Difference Root Mean

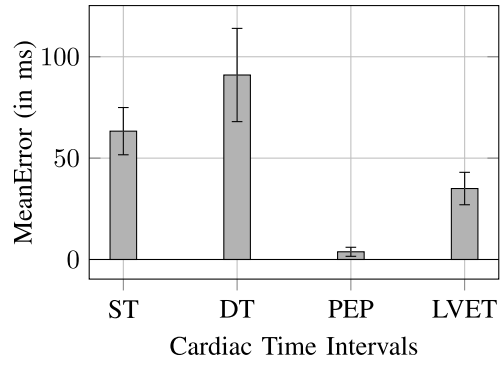

Fig. 10. Accuracy evaluation results of Cardiac Time Intervals with respect to MeanError for the test dataset.

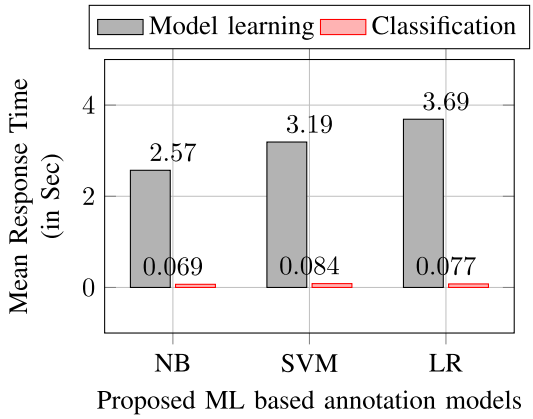

Fig. 11. The responsiveness evaluation results with respect to the Mean Response Time (MeanRT) for the testing dataset.

Square Error (TDRMSE) is also calculated for each desired SCG peak as shown in Fig. 9. From Fig. 9, it can be observed that MC and AO has the maximum and minimum TDRMSE, respectively.

3) Results of Cardiac Time Intervals Estimation: Apart from the qualitative accuracy evaluation of the desired SCG peaks, the accuracy assessment of Cardiac Time Intervals (CTIs), one of the important aspects of Cardiac Health Parameters (CHPs) is also performed. The CTIs such as ST, DT, PEP, and $LVET$ are estimated for $MeanError \pm SD$ as shown in Fig. 10. It is clear from Fig. 10 that the MeanError between the manual and proposed classifier is insignificant, which shows the efficient estimation of CTIs. Moreover, Fig. 10 shows that MeanError in the estimation of the systolic time interval is less as compared to that of the diastolic time interval.

4) Results of Classifier Responsiveness: In addition to the quantitative and qualitative accuracy evaluations, the proposed annotation models are also evaluated to know their responsiveness for model learning and classification of each peak in a CC as shown in Fig. 11. As it can be seen in Fig. 11, among the aforementioned proposed annotation models, NB takes the least amount of time to learn as well as classify the desired SCG peaks. On the contrary, the SVM and LR takes the maximum amount of classification and model learning time, respectively.

VII. Discussion

The performance of expert annotation is not uniform across the SCG peaks. As shown in Fig. 5, it is observed that IM, AO, IC, and RE are successfully annotated in significant number of training CCs compared to AS, MC, AC, MO, and RF. The potential explanation for the successful annotation of AO in most training CCs is its distinctive property of high $+ve$ amplitude as shown in Fig. 1, which makes it easy for the expert annotators to identify and annotate it. On the contrary, peaks AS, MC, AC, MO, and RF usually exhibit low amplitude with similar morphological characteristics to that of other closely appearing candidate peaks as shown in Fig. 1, which makes them more difficult to annotate.

The annotation results shown in Fig. 6 indicates that the proposed binary classifiers consistently follows the annotation trend of expert annotation. Based on the results, it is argued that binary classifiers are the suitable alternative to address the SCG annotation problem. The results of Fig. 7 justifies our claim. The limited performance improvement of the conventional approaches can be explained as follow. The Env_SCG [11] generates external envelopes to mask the SCG signals and locate the IM, AO, and AC. This helps Env_SCG [11] to improve the accuracy of annotation. However, Env_SCG [11] considers the fixed window size, which saturates the accuracy improvement. On the contrary, $Sliding\_SCG$ [19] dynamically adjust the window size and outperforms $basline$ and proposed NB_S_{SCGPs}. However, $Sliding\_SCG$ [19] lacks the method to locate the probable search area for the identification of peaks. The results of Fig. 7 show that the proposed classifier LR_S_{SCGPs} consistently outperforms the Env_SCG [11], $Sliding\_SCG$ [19], and $baseline$. Moreover, the results of SVM_S_{SCGPs} are comparable to the Env_SCG [11] and $Sliding\_SCG$ [19].

The significant advantage of the proposed approach is the process of zone formation, which eliminates the need for a fixed-size sliding window as required by conventional approaches. The zones are formed following a simple process of ECG alignment, which results in significant improvement of the accuracy with negligible overhead. Besides, the proposed approach has derived distinctive properties that help to reduce the search area, which subsequently improves the chances of accurate peak annotation. Different from conventional approaches, the proposed approach continuously learns the morphological characteristics of signals to dynamically tune the features, which help annotate fluctuating SCG signals across the cardiac cycles.

The potentials reason for the marginal decrease in the performance of NB and SVM is as follows. The NB is a probabilistic classifier and mainly suffers due to its inherent assumption of conditional independence among the features. On the contrary, in many instances, SVM tends to wrongly classify peaks near to classification hyperplane due to external noise induce input signals. It is to note that the proposed classifiers consistently perform better and provide satisfactory results with respect to the expert annotation.

The fundamental reason for having the least Mean Response Time (MeanRT) for NB is its linear time estimation for Maximum-likelihood training. It is to be noted that the machine learning-based annotation models learning is a one time process, following which classification can be performed repeatedly for each SCG peak. Once the annotation models are trained, the time to classify the peaks is observed in the the fraction of $\frac{1}{10}$ of a second, which implies that all of the annotation models are fast enough to be considered for the real-time monitoring and continuous estimation of CHPs from the unobtrusive SCG signals.

VIII. Conclusion and Future Work

In this paper, automatic annotation of SCG signals is explored for the application in real-time cardiac healthcare monitoring. Unlike previous studies, the proposed study employs machine learning models to automate the annotation over the traditional approaches. The annotation process is expedited by formulating the knowledge-based representative rules and distinctive properties derived from the SCG morphology. Besides, ensemble features are designed for the robust identification of the desired SCG peaks. The experimental results reveal that annotation accuracy noticeably improves over recent state-of-the-art alternatives. However, there are a few limitations. The proposed SCG annotation scheme is dependent on the concurrent ECG signals and the classifiers are built on the top of three simple features to make the system suitable for real-time monitoring. Only the selected classifiers are chosen for the annotation to avoid computational complexity. However, we argue that the annotation accuracy can be further improved in two ways. 1). By incorporating the more complex features based on the signal morphology and beat-to-beat correlation. 2). By employing computationally expensive machine learning algorithms such as recurrent neural networks etc. In the future, we starve to design computationally inexpensive yet robust learning models that annotate the SCG without the need for concurrent ECG signals. Further, we intend to extend our work by experimenting with the inclusion of the complex features.

References

[1] Z. Xia, M. M. H. Shandhi, O. T. Inan, and Y. Zhang, "Non-contact sensing of seismocardiogram signals using microwave Doppler radar," *IEEE Sensors J.*, vol. 18, no. 14, pp. 5956–5964, Jul. 15, 2018.

[2] A. Taebi, B. E. Solar, A. J. Bomar, R. H. Sandler, and H. A. Mansy, "Recent advances in seismocardiography," *Vibration*, vol. 2, no. 1, pp. 64–86, 2019.

[3] M. Di Rienzo, E. Vaini, and P. Lombardi, "Development of a smart garment for the assessment of cardiac mechanical performance and other vital signs during sleep in microgravity," *Sens. Actuators A, Phys.*, vol. 274, pp. 19–27, May 2018.

[4] K. Sørensen, S. E. Schmidt, A. S. Jensen, P. Søgaard, and J. J. Struijk, "Definition of fiducial points in the normal seismocardiogram," *Sci. Rep.*, vol. 8, no. 1, p. 15455, 2018.

[5] K. Tavakolian, G. A. Dumont, G. Houlton, and A. P. Blaber, "Precordial vibrations provide noninvasive detection of early-stage hemorrhage," *Shock*, vol. 41, no. 2, pp. 91–96, 2014.

[6] M. Kaisti *et al.*, "Stand-alone heartbeat detection in multidimensional mechanocardiograms," *IEEE Sensors J.*, vol. 19, no. 1, pp. 234–242, Jan. 1, 2019.

[7] M. Becker *et al.*, "Simplified detection of myocardial ischemia by seismocardiography," *Herz*, vol. 39, no. 5, pp. 586–592, 2014.

[8] O. Faust, Y. Hagiwara, T. J. Hong, O. S. Lih, and U. R. Acharya, "Deep learning for healthcare applications based on physiological signals: A review," *Comput. Methods Programs Biomed.*, vol. 161, pp. 1–13, Jul. 2018.

[9] O. T. Inan *et al.*, "Ballistocardiography and seismocardiography: A review of recent advances," *IEEE J. Biomed. Health Informat.*, vol. 19, no. 4, pp. 1414–1427, Jul. 2015.

[10] H. Ashouri, S. Hersek, and O. T. Inan, "Universal pre-ejection period estimation using seismocardiography: Quantifying the effects of sensor placement and regression algorithms," *IEEE Sensors J.*, vol. 18, no. 4, pp. 1665–1674, Feb. 15, 2018.

[11] F. Khosrow-Khavar, K. Tavakolian, A. Blaber, and C. Menon, "Automatic and robust delineation of the fiducial points of the seismocardiogram signal for noninvasive estimation of cardiac time intervals," *IEEE Trans. Biomed. Eng.*, vol. 64, no. 8, pp. 1701–1710, Aug. 2017.

[12] V. Zakeri, A. Akhbardeh, N. Alamdari, R. Fazel-Rezai, M. Paukkunen, and K. Tavakolian, "Analyzing seismocardiogram cycles to identify the respiratory phases," *IEEE Trans. Biomed. Eng.*, vol. 64, no. 8, pp. 1786–1792, Aug. 2017.

[13] P. K. Sahoo, H. K. Thakkar, W.-Y. Lin, P.-C. Chang, and M.-Y. Lee, "On the design of an efficient cardiac health monitoring system through combined analysis of ECG and SCG signals," *Sensors*, vol. 18, no. 2, p. 379, 2018.

[14] P. K. Sahoo, H. K. Thakkar, and M.-Y. Lee, "A cardiac early warning system with multi channel SCG and ECG monitoring for mobile health," *Sensors*, vol. 17, no. 4, p. 711, 2017.

[15] T. Choudhary, L. N. Sharma, and M. K. Bhuyan, "Automatic detection of aortic valve opening using seismocardiography in healthy individuals," *IEEE J. Biomed. Health Inform.*, vol. 23, no. 3, pp. 1032–1040, May 2019.

[16] Y. D'Mello *et al.*, "Autocorrelated differential algorithm for real-time seismocardiography analysis," *IEEE Sensors J.*, vol. 19, no. 13, pp. 5127–5140, Jul. 1, 2019.

[17] N. Mora, F. Cocconcelli, G. Matrella, and P. Ciampolini, "Fully automated annotation of seismocardiogram for noninvasive vital sign measurements," *IEEE Trans. Instrum. Meas.*, to be published.

[18] F. Khosrow-Khavar, K. Tavakolian, A. P. Blaber, J. M. Zanetti, R. Fazel-Rezai, and C. Menon, "Automatic annotation of seismocardiogram with high-frequency precordial accelerations," *IEEE J. Biomed. Health Inform.*, vol. 19, no. 4, pp. 1428–1434, Jul. 2015.

[19] G. Shafiq, S. Tatinati, W. T. Ang, and K. C. Veluvolu, "Automatic identification of systolic time intervals in seismocardiogram," *Sci. Rep.*, vol. 6, no. 1, p. 37524, Dec. 2016.

[20] C. Yang, S. Tang, and N. Tavassolian, "Annotation of seismocardiogram using gyroscopic recordings," in *Proc. IEEE Biomed. Circuits Syst. Conf. (BioCAS)*, Oct. 2016, pp. 204–207.

[21] R. Crow, P. Hannan, D. Jacobs, L. Hedquist, and D. M. Salerno, "Relationship between seismocardiogram and echocardiogram for events in the cardiac cycle," *Amer. J. Noninvasive Cardiol.*, vol. 8, no. 1, pp. 39–46, 1994.

[22] J. R. Mitchell and J.-J. Wang, "Expanding application of the Wiggers diagram to teach cardiovascular physiology," *Adv. Physiol. Educ.*, vol. 38, no. 2, pp. 170–175, 2014.

[23] M. A. García-González, A. Argelagós-Palau, M. Fernández-Chimeno, and J. Ramos-Castro, "A comparison of heartbeat detectors for the seismocardiogram," in *Proc. Comput. Cardiol.*, Sep. 2013, pp. 461–464.

[24] A. L. Goldberger *et al.*, "Physiobank, physiotoolkit, and physionet: Components of a new research resource for complex physiologic signals," *Circulation*, vol. 101, no. 23, pp. e215–e220, 2000.

[25] T. Choudhary, L. N. Sharma, and M. K. Bhuyan, "Heart sound extraction from sternal seismocardiographic signal," *IEEE Signal Process. Lett.*, vol. 25, no. 4, pp. 482–486, Apr. 2018.

[26] J. Sim and C. C. Wright, "The kappa statistic in reliability studies: Use, interpretation, and sample size requirements," *Phys. Therapy*, vol. 85, no. 3, pp. 257–268, 2005.

[27] F. Pedregosa *et al.*, "Scikit-learn: Machine learning in Python," *J. Mach. Learn. Res.*, vol. 12, pp. 2825–2830, Oct. 2011.

Hiren Kumar Thakkar (M'19) received the M.Tech. degree from the Department of Computer Science and Engineering, IIIT Bhubaneswar, Bhubaneswar, India, in 2012, and the Ph.D. degree from the Department of Computer Science and Information Engineering, Chang Gung University, Taiwan, in 2018. He is currently an Assistant Professor with the Department of Computer Science Engineering, Bennett University, India. His research interests include the areas of bio-medical big data analysis, cloud resource management and optimization, and applied machine learning.

Prasan Kumar Sahoo (SM'16) received the B.Sc. degree (Hons.) in physics, the M.Sc. degree in mathematics from Utkal University, Bhubaneswar, India, in 1987 and 1994, respectively, the M.Tech. degree in computer science from the Indian Institute of Technology (IIT), Kharagpur, India, in 2000, the first Ph.D. degree in mathematics from Utkal University, in 2002, and the second Ph.D. degree in computer science and information engineering from National Central University, Taiwan, in 2009. He was an Associate Professor with the Department of Information Management, Vanung University, Taiwan, from 2007 to 2011. He was a Visiting Associate Professor with the Department of Computer Science, Universite Claude Bernard Lyon 1, France. He has been an Adjunct Researcher with the Division of Colon and Rectal Surgery, Chang Gung Memorial Hospital, Linkou, Taiwan, since 2018. He is currently a Professor with the Department of Computer Science and Information Engineering, Chang Gung University, Taiwan. His current research interests include artificial intelligence, big data analytic, cloud computing, and IoT. He was a program committee member of several IEEE and ACM conferences. He is an Editorial Board Member for the *International Journal of Vehicle Information and Communication Systems*.